XLI CILAMCE
XLI Ibero-Latin American Congress on Computational Methods in Engineering
16-19 November, 2020 FOZ DO IGUAÇU PARANÁ - BRAZIL

Bayesian statistics of uncertainty quantification attenuation bands of three-dimensional phononic lattices

L. H. M. S. Ribeiro[1], V. F. Dal Poggetto[2], D. Beli[3], A. T. Fabro[4], J. R. F. Arruda[1]

[1]*School of Mechanical Engineering, University of Campinas*
Rua Mendeleyev, 200, Campinas-SP, 13083-860, Brazil
luiz.marra@outlook.com, arruda@fem.unicamp.br
[2]*Department of Civil, Environmental and Mechanical Engineering, University of Trento*
Laboratory of Bio-inspired, Bionic, Nano and Meta Materials & Mechanics, Trento, 38123, Italy
v.fonsecadalpoggetto@unitn.it
[3]*São Carlos School of Engineering, University of São Paulo*
Avenida João Dagnone, 1100. São Carlos-SP, 13563-120, Brazil
beli.danilo@gmail.com
[4]*Department of Mechanical Engineering, University of Brasilia*
Rua Via L3 Norte, Brasilia-DF, 70910-900, Brazil
fabro@unb.br

Abstract. Phononic crystals are periodic structures that may present Bragg scattering and wave coupling band gaps, which are frequency ranges where waves cannot propagate freely. In this work, it is proposed a three-dimensional frame structure that can be used to support and isolate vibrations of a rigid payload. This structure is a 3D lattice made of frame elements. Firstly, one frame presenting the intersection of longitudinal, flexural, and torsional band gaps were proposed. The resulting unit cell is modeled via the spectral element method (SEM). The three-dimensional structural model includes constraints and inertial characteristics of a rigid body attached at its top. Pseudo experiments are performed using mechanical property values sampled from previously defined statistical distributions. A Markov chain Monte Carlo (MCMC) algorithm is used to estimate posterior distributions of mechanical properties considered as statistical variables. Prony's method is used in the MCMC algorithm to improve its precision. The Monte Carlo method is used to infer about the stochastic wavenumber. Two robust and complete attenuation bands related to the considered variability are observed, which are shown on the dispersion diagram of the 3D structure for some observations along the contours of the irreducible Brillouin zone (IBZ). Such attenuation bands can also be observed on the forced response of the rigid payload subjected to base excitations.

Keywords: Three-dimensional wave propagation, Phononic crystal, Uncertainty quantification, Periodic structure, Vibration passive control

1 Introduction

Studies on three-dimensional periodic structures show they may present interesting phenomena such as Bragg scattering, veering and locking coupling band gaps, and therefore work as passive vibration control devices [1–3].

The wave propagation approach has some advantages, when dealing with periodic structures, such as the physical interpretation for wave related phenomena, with a reduced computational cost [3–6].

Additive manufacturing made it possible to design more complex periodic structures. However, mechanical property variability is substantial for such manufacturing processes and should be considered [4, 7]. Statistical methods have been developed to quantify uncertainties related to variability of the considered parameters [8, 9] and the Bayesian approach has presented good results for structural problems [6, 10–12].

The objective of the present study is to present a methodology that uses Bayesian statistics to infer the mechanical properties and the stochastic response of a periodic structure. A periodic three-dimensional phononic crystal (PC) unit cell is proposed, and a built up finite structure is designed using this unit cell. The stochastic response is obtained from the unit cell. The deterministic response of the built up structure were obtained using the mechanical property mean values to better understand the nature of the observed attenuation bands.

2 Methodology

2.1 Wave propagation approach

Using Hamilton's principle, it is possible to obtain the equations of motion of the one-dimensional elementary rod, Saint-Venant's shaft, and Timoshenko beam [13–17]:

$$\frac{\partial}{\partial x}\left(EA\frac{\partial u_x}{\partial x}\right) - \rho A\frac{\partial^2 u_x}{\partial t^2} = q_n(x); \quad (1) \qquad \frac{\partial}{\partial x}\left(GK_s\frac{\partial \phi_x}{\partial x}\right) - \rho J\frac{\partial^2 \phi_x}{\partial t^2} = q_t(x), \quad (2)$$

$$GA\kappa\left(\frac{\partial^2 v_y}{\partial x^2} - \frac{\partial \phi_z}{\partial x}\right) - \rho A\frac{\partial^2 v_y}{\partial t^2} = q_v(x), \quad \frac{\partial}{\partial x}\left(EI\frac{\partial \phi_z}{\partial x}\right) + GA\kappa\left(\frac{\partial v_y}{\partial x} - \phi_z\right) - \rho I\frac{\partial^2 \phi_z}{\partial t^2} = q_m(x); \quad (3)$$

where the mechanical properties E, ρ, and G are, respectively, the material Young's modulus, mass density, and shear modulus, the geometric properties A, I, K_s, ρJ , and κ are, respectively, the element cross-sectional area, second moment of area, torsion constant (Saint-Venant's correction due the non-circularity of the shaft), mass moment of inertia per unit of length, and Timoshenko shear coefficient, the quantities u_x, v_y, ϕ_z, ϕ_x, $q_n(x)$, $q_v(x)$, $q_m(x)$, and $q_t(x)$ are, respectively, the element longitudinal and transversal displacements, the beam shear deformation angle, the torsional angle, and the rod, beam (transverse and rotational), and shaft external loads.

Using Equations (1) (2), and (3) for each structural element, it is possible to obtain the analytical solution of a frame with constant mechanical and geometric properties for the whole length of each one-dimensional element. Also, it is possible to obtain the beam, rod, and shaft dynamic stiffness matrices via the spectral element method, which relates displacements and forces in the frequency domain [15]:

$$\boldsymbol{D}_c(\omega)\mathbf{q} = \mathbf{F}. \quad (4)$$

The spectral elements of beam, rod, and shaft can be assembled as a three-dimensional frame element [18]. This element has constant mechanical and geometric properties throughout its length. Hence, a structure with varying properties can be divided into a defined number of elements, which can be assembled similarly to the finite element method (FEM) [18] and, considering internal nodes free of external forces, a condensation process can be applied to consider only two nodes, located at their edges [19].

Six elements (e_i, $i = 1, \ldots, 6$) with properties varying throughout their length (L) can be modeled via SEM, and then assembled as schematically represented in Figure 1a. Hence, node $\mathbf{q}_7$ can be condensed considering there are no external forces applied there, keeping only the external nodes ($\mathbf{q}_1, \ldots, \mathbf{q}_6$) at the three-dimensional unit cell.

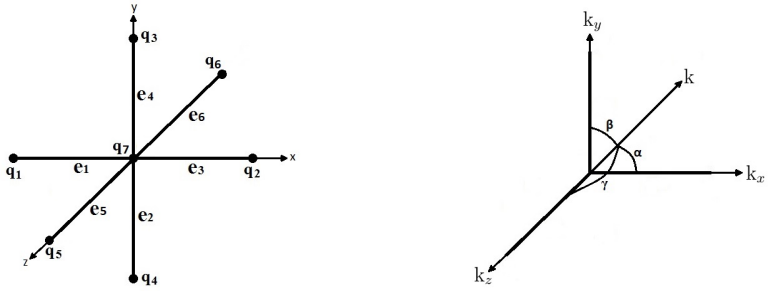

(a) Schematic representation of the three-dimensional unit cell.

(b) Decomposition of k into its Cartesian components.

Figure 1. Schematic representation of the three-dimensional unit cell and Cartesian decomposition of k.

Using the Bloch-Floquet theorem [20, 21], and considering the proposed Cartesian system, we have $\mathbf{q}_2 = \lambda_x^2\mathbf{q}_1$, $\mathbf{q}_3 = \lambda_y^2\mathbf{q}_4$, and $\mathbf{q}_5 = \lambda_z^2\mathbf{q}_6$. Hence, it is possible to write $\mathbf{q}_1, \ldots, \mathbf{q}_6$ related to $\mathbf{q}_1$ only [11, 22]:

$$\begin{Bmatrix}\mathbf{q}_1 & \mathbf{q}_2 & \mathbf{q}_3 & \mathbf{q}_4 & \mathbf{q}_5 & \mathbf{q}_6\end{Bmatrix}^t = \begin{bmatrix}\mathbf{I}_n & \mathbf{I}_n\lambda_x^2 & \mathbf{I}_n\lambda_x\lambda_y & \mathbf{I}_n\lambda_x\lambda_y^{-1} & \mathbf{I}_n\lambda_x\lambda_z & \mathbf{I}_n\lambda_x\lambda_z^{-1}\end{bmatrix}^t \mathbf{q}_1 \quad \rightarrow \quad \mathbf{q} = \boldsymbol{\Lambda}_R\mathbf{q}_1. \quad (5)$$

where $\lambda_x = e^{-ik_xL_x}$, $\lambda_y = e^{-ik_yL_y}$, and $\lambda_z = e^{-ik_zL_z}$. Moreover, it is possible to use the equilibrium of the external forces using the matrix relation:

$$\begin{bmatrix}\boldsymbol{I}_n & \boldsymbol{I}_n\lambda_x^{-2} & \boldsymbol{I}_n\lambda_x^{-1}\lambda_{yj}^{-1} & \boldsymbol{I}_n\lambda_x^{-1}\lambda_y & \boldsymbol{I}_n\lambda_x^{-1}\lambda_z^{-1} & \boldsymbol{I}_n\lambda_x^{-1}\lambda_z\end{bmatrix}\begin{Bmatrix}\mathbf{F}_1 & \mathbf{F}_2 & \mathbf{F}_3 & \mathbf{F}_4 & \mathbf{F}_5 & \mathbf{F}_6\end{Bmatrix}^t = \boldsymbol{\Lambda}_L\begin{Bmatrix}\mathbf{F}\end{Bmatrix} = \mathbf{0}. \quad (6)$$

Now, substituting Equation (5) in Equation (4) and premultiplying both sides by $\mathbf{\Lambda}_L$ one obtains:

$$\mathbf{\Lambda}_L \mathbf{D}_c(\omega) \mathbf{\Lambda}_R \mathbf{q}_1 = \mathbf{0}, \tag{7}$$

which is a polynomial problem with roots λ_{xj}, λ_{yj}, and λ_{zj}.

The wavenumber k can be decomposed using its Cartesian components into k_x, k_y, and k_z as represented in Figure 1b. Wavenumber values k_y and k_z can be related to k_x, α, and β, or in exponential terms, where λ_x, λ_y and λ_z are related using:

$$\begin{aligned} k_y &= \frac{cos(\beta)}{cos(\alpha)} k_x, \\ k_z &= \frac{\sqrt{1 - cos^2(\alpha) - cos^2(\beta)}}{cos(\alpha)} k_x, \end{aligned} \tag{8}$$

$$\begin{aligned} \lambda_y &= \lambda_x^{\frac{cos(\beta)}{cos(\alpha)} \frac{L_y}{L_x}}, \\ \lambda_z &= \lambda_x^{\frac{\sqrt{1-cos^2(\alpha)-cos^2(\beta)}}{cos(\alpha)} \frac{L_z}{L_x}}. \end{aligned} \tag{9}$$

If $\frac{cos(\beta)}{cos(\alpha)} \frac{L_y}{L_x}$ and $\frac{\sqrt{1-cos^2(\alpha)-cos^2(\beta)}}{cos(\alpha)} \frac{L_z}{L_x}$ are integers simultaneously, the polynomial equation indicated in Equation (7) will increase its order, but remains an ordinary polynomial than can be solved using its companion matrix [11, 22].

By this approach, it is possible to obtain the dispersion relation scanning the first Brillouin zone (FBZ) represented in Figure 2a [3]. In addition, as the elementary cell (Figure 1a) is symmetric with respect to the axes x, y, and z, it is necessary to scan only the IBZ to check for a complete band gap [23]. As presented in Figure 2a, the contour of the IBZ consists of four parts: from $\mathbf{\Gamma}$ to $\mathbf{X}$, where $\gamma = 0°$, $\beta = 90°$ and $\alpha = 90°$ (k_1); from $\mathbf{X}$ to $\mathbf{M}$, where $\beta = 90°$, α varies from $90°$ to $135°$ and γ varies from $0°$ to $45°$; from $\mathbf{M}$ to $\mathbf{R}$, where α is $135°$, γ is $45°$, and β varies from $90°$ to $45°$; and from $\mathbf{R}$ to $\mathbf{\Gamma}$, where α is $135°$, γ is $45°$, and β is $45°$ (k_7).

However, in order to maintain the polynomial ordinary and reduce computational cost, three observations were taken at the IBZ from $\mathbf{X}$ to $\mathbf{M}$ ($\gamma = 63.435°$ and $\beta = 108.435°$, $\gamma = 75.964°$ and $\beta = 120.964°$, and $\gamma = 90°$ and $\beta = 135°$) named, receptively k_2, k_3 and k_4; and from $\mathbf{M}$ to $\mathbf{R}$: ($\beta = 63.435°$; and $\beta = 75.964°$) named, respectively, k_5 and k_6 as represented in Figure 2b.

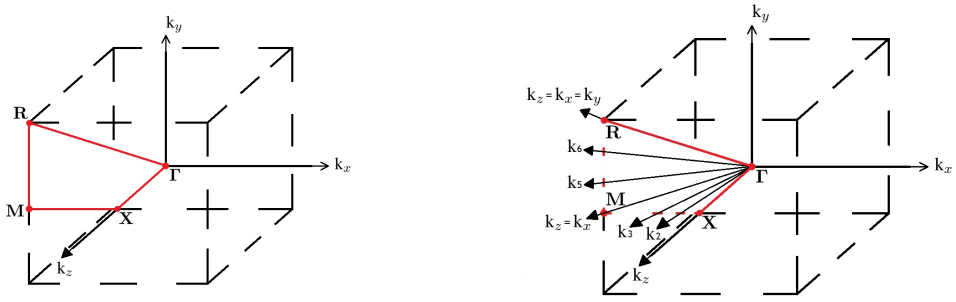

(a) Representation of the FBZ and IBZ (red) in the reciprocal space for the three-dimensional unit cell.

(b) Representation of the samples made in the contour line $\mathbf{X} - \mathbf{M}$ and $\mathbf{M} - \mathbf{R}$ in the IBZ for the three-dimensional unit cell.

Figure 2. Representation of the IBZ for the proposed three-dimensional structure (a), and the proposed observations along the contour line from $\mathbf{X}$ to $\mathbf{M}$ and from $\mathbf{M}$ to $\mathbf{R}$ (b).

For given values of β, γ, and α, the polynomial on Equation (7) may yield a large number of wavenumbers, (k_2 can yield 96 different wavemodes) but most of them have no physical meaning [22]. Modes with physical meaning are here named principal modes, which can be selected by including a perturbation in the mathematical model, and keeping the more robust modes [22]. This procedure can be computationally expensive [6, 11].

The imaginary part of the complex wavenumber represents the evanescent part of the wave for a given frequency [6]. Hence, the minimum value of $\mid \mathrm{Im}(k) \mid$, can be a meaningful evidence of a complete and full attenuation band if, for all the observations in the IBZ, all wavenumbers present δ_m greater than a defined value of attenuation (in percentage), where δ_m is the attenuation per cell given by [6]:

$$\delta_m = 100(1 - e^{-\mathrm{Im}(k)}). \tag{10}$$

This methodology facilitates the calculation of attenuation bands, especially for the stochastic result, where the response has to be computed several times according to the proposed methodology that represents the variability, which is usually observed due to the manufacturing process [4, 24].

2.2 Uncertainty quantification of the mechanical property variability

First, a Gamma distribution is proposed for the statistical mechanical properties (E and ρ). It is made via the maximum likelihood estimator, applied to some observed valued reported in the literature. Eight pairs of values were sampled from each distribution and those values were considered as observations (details in [10].)

In order to estimate the distributions of E and ρ, an MCMC algorithm was proposed in a way that it uses an informative prior distribution, the likelihood function, and Prony's method to obtain the posterior distribution. Using each pair of E and ρ, one periodic beam was simulated, where FRF values were simulated throughout the frame. Using Prony's method, which has its peculiarities described in [24], the equivalent wavenumbers are estimated. Then, a mean error between the estimated wavenumber and the value from the model inside the MCMC algorithm for a frequency range is used to improve the algorithm precision.

After inferring the distributions of E and ρ, considering the Poisson's ratio (ν) constant, the shear modulus G can be obtained as a random variable using the relation $G = \frac{E}{2(1+\nu)}$.

There are three methods widely used to check the MCMC chain convergence [25] already implemented in the R package "coda" [26]: Geweke's criterion ($|$ZG$|$), the Heidelberger and Welch test (HW-p), and the Raftery and Lewis (1992) factor (RL).

The posterior distribution and the expansion optimal linear estimator (EOLE) [27] were used to represent the spatial variability of the mechanical properties as stochastic fields that were decomposed into an eigenvalues and eigenvectors when discretized [6, 11] similarly to the discrete Karhunen–Loève (KL) expansion [28].

Finally, the Monte Carlo method was used to run this procedure, sampling from the posterior distribution according to the spatial discretization, expanding and smoothing the spatial field of the parameters E and ρ using EOLE as the convergence of the Monte Carlo method requires [14]. Afterwards, the Bayes' factor (BF) was used to infer on the stochastic response (the minimum of $\mid \mathrm{Im}(k) \mid$ from k_1 to k_7) [6, 11]. The BF, in practice, can be interpreted as a ratio of chanced against or in favor of the null hypotheses [29]. In the present application, if the curve representing the BF is greater then zero, it represents that there is a chance equal to or greater to the BF value in favor of the occurrence of the attenuation band.

2.3 Obtaining the forced response for the complete structure

To apply the proposed approach to a feasible structure, a built up structure made of 4 three-dimensional cells is proposed. In addition, a plate structure was assembled at the top of the periodic frame structure, and the lower DOFs were allowed to displace vertically only [30]. Therefore, the constraint due to the plate, as well as its rotational inertia and mass were modeled at the top of the frame. The FRF obtained using the mean values of the posterior distributions were compared with the deterministic response in the form of attenuation bands obtained from the deterministic three-dimensional unit cell using the same mean values.

3 Results

In this section, we present the results in the following order: the posterior distributions, deterministic analysis using the mean values, and the stochastic analysis on the dispersion diagram.

3.1 Posterior distributions

The mechanical property posterior distributions obtained via the proposed MCMC algorithm yields the distributions presented in Figure 3, and and its convergence tests were also checked:

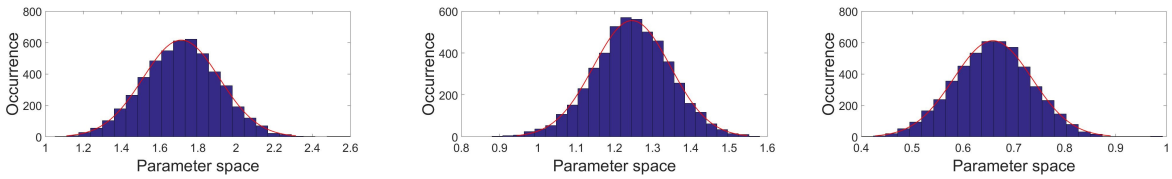

(a) Posterior distribution of E (red line) and histogram.

(b) Posterior distribution of ρ (red line) and histogram.

(c) Posterior distribution of G (red line) and histogram.

Figure 3. Estimated posterior distributions.

3.2 Deterministic results

Considering the unit cell with length of 43.6 mm and a cross-shaped cross-section with a profile given by the following expression:

$$h(x) = \frac{0.015}{(e^{(8.25-700x)}+1)}, \qquad 0 \leq x \leq 0.0218, \qquad h(0.0218+x) = h(0.0218-x), \tag{11}$$

where $h(x)$ is symmetric with respect to $x = 0.0218$ m with maximum value at $x = 0.0218$ m of 15 mm, it is possible to assemble the three-dimensional cell schematically represented by Figure 1a and whose design if presented by Figure 4.

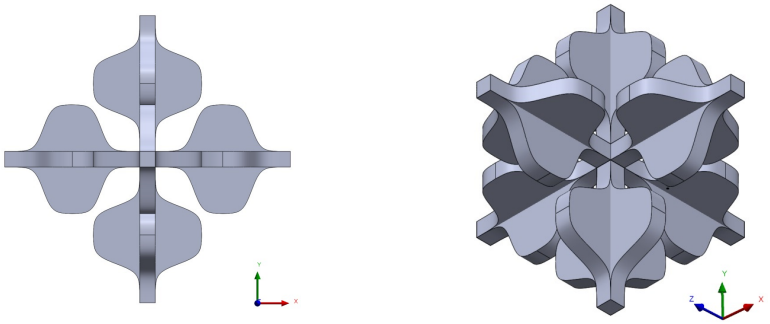

(a) Front view of proposed three-dimensional unit cell.

(b) Isometric view of proposed three-dimensional unit cell.

Figure 4. Proposed three-dimensional unit cell.

Figure 5 represents the response for the minimum value of $|\ \mathrm{Im}(k)\ |$ for the seven wavenumber combinations. In the present study, three gray color patches are used for $\delta = 0.2$, $\delta = 1.1$, and $\delta = 1.35$. Those values were defined to indicate attenuations of, respectively and approximately, at least 18% ($\delta_c \geq 0.18$), 67% ($\delta_c \geq 0.67$), and 74% ($\delta_c \geq 0.74$) per cell length. It is possible to observe that the main attenuation band is located between 12 and 17 kHz for $\delta_c \geq 0.74$ and between 9 and 18 kHz for $\delta_c \geq 0.67$.

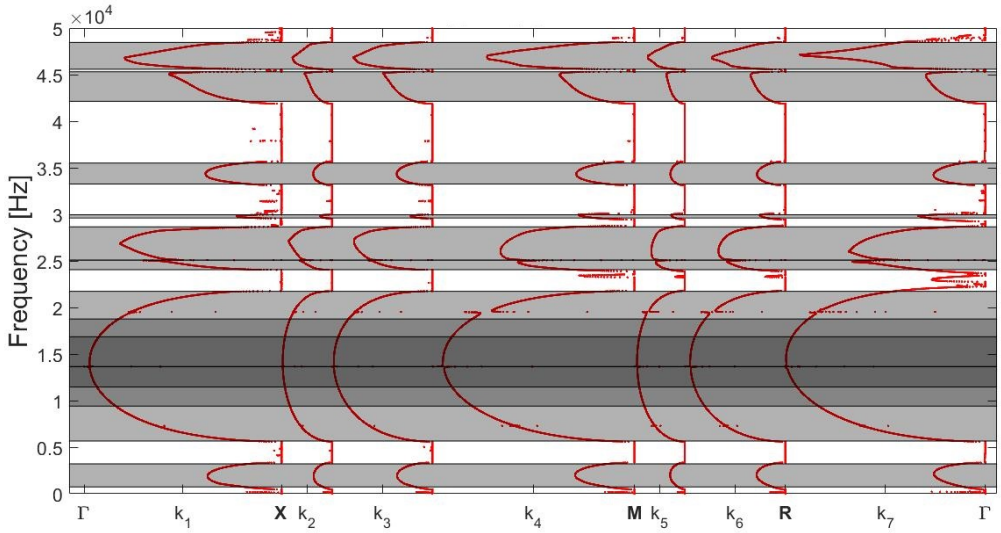

Figure 5. Minimum of the magnitude of the imaginary part of the wavenumber for the samples along the contour of the IBZ for the cell represented in Figure 4 from 0 to 50 kHz. Attenuation of at least 18% ($\delta_c \geq 0.18$; light gray), 67% ($\delta_c \geq 0.67$; middle gray), and 74% ($\delta_c \geq 0.74$; dark gray) per cell length.

3.3 Forced response for the proposed support

Figure 7 shows the simulated complete structure (front view in Figure 7a and isometric view in Figure 7b) for the computation of the FRF via exciting all the lower nodes (y direction) and measuring the response at the top

nodes (y direction), which are presented in Figure 6, where it is possible to verify a good agreement, especially for the main band gap (9-18 kHz) between the dispersion response from the three-dimensional unit cell and the dynamic response for the whole structure, except for some modes within the band gaps, which could be caused by defects or local resonances.

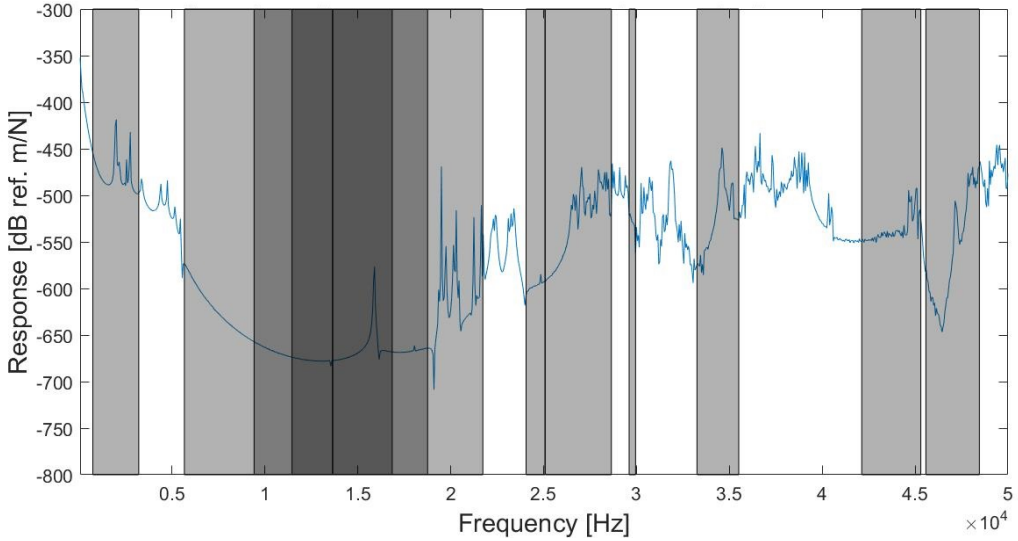

Figure 6. FRF obtained from the proposed complete structure (Figure 7) from 0 to 50 kHz. Attenuation of at least 18% ($\delta_c \geq 0.18$; light gray), 67% ($\delta_c \geq 0.67$; middle gray), and 74% ($\delta_c \geq 0.74$; dark gray) per cell length.

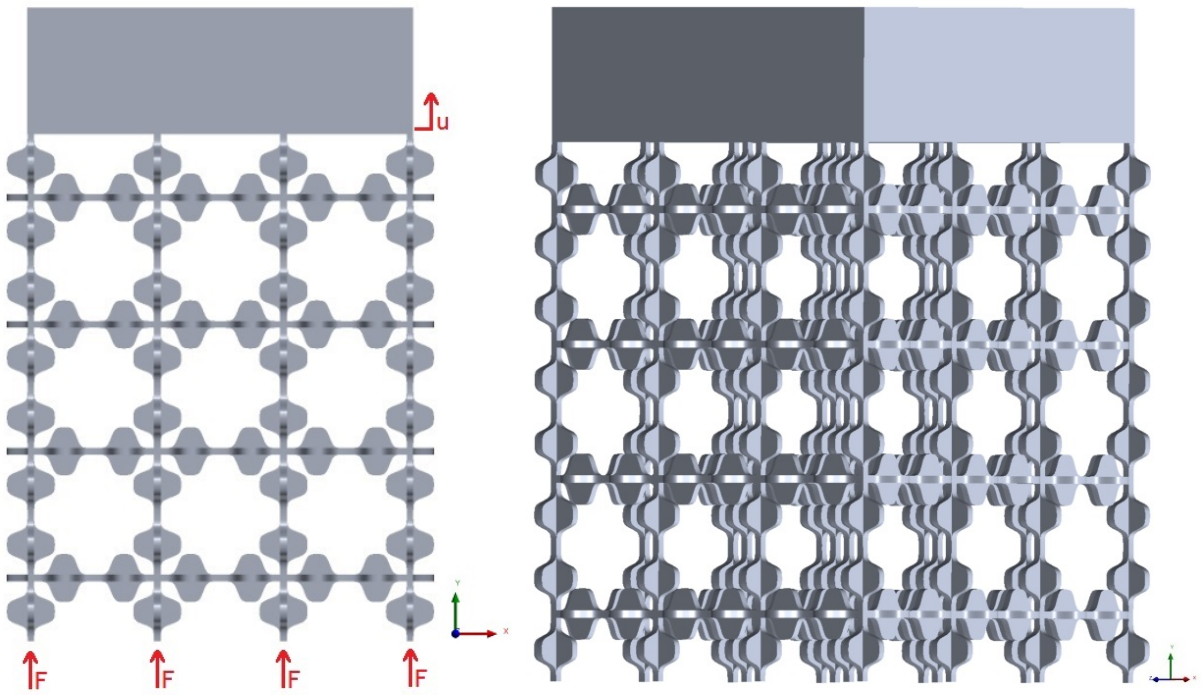

(a) Front view of the proposed complete structure.

(b) Isometric view of the proposed complete structure.

Figure 7. Proposed structure, as a support for a solid payload at the top nodes, where all the nodes at the base are excited in vertical direction. The response is the measurement made at the top nodes.

3.4 Stochastic results

Stochastic wavenumber (the minimum of $|\ \mathrm{Im}(k)\ |$), which relates to the minimum attenuation for all waves (longitudinal, flexural and torsional), for $\mathrm{k}_1, \ldots, \mathrm{k}_7$ after 1,000 steps of the Monte Carlo method. We applied the

BF to infer on this stochastic response. For instance, where the line is marked in cyan, there is 100 times more chance of existing an attenuation band than not existing. Figure 8 presents two different patches related to the minimum attenuation of at least 18% per cell ($\delta_c \geq 0.18$, light gray), and of at least 67% per cell ($\delta_c \geq 0.67$, dark gray) throughout the IBZ. Two different attenuation bands were observed: the first one, at low frequency range (0.5-3 kHz), of at least 18% per cell, and the second one at higher frequencies presented regions of at least 67% per cell (10-17.5 kHz).

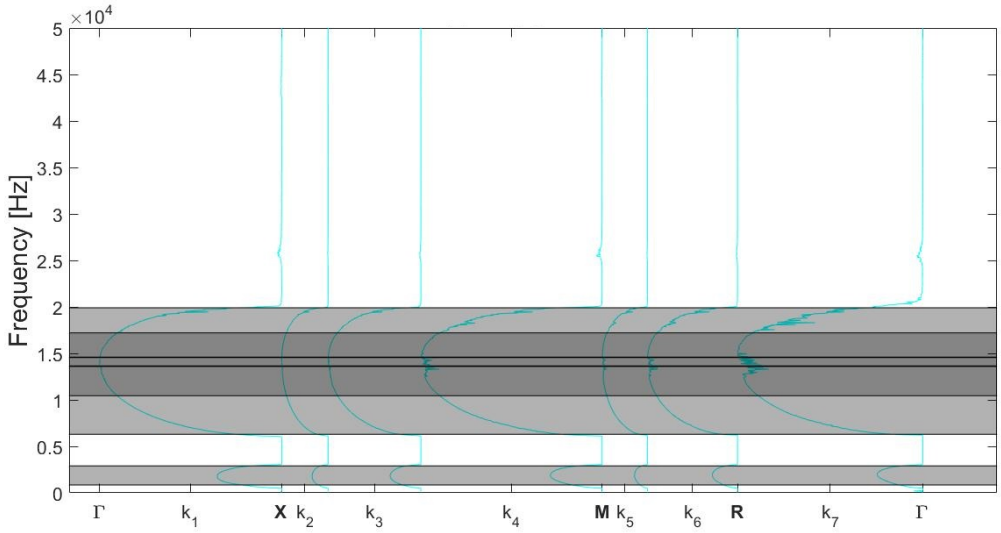

Figure 8. Minimum value of the magnitude of the imaginary part for BF100 for the proposed valued of θ from 0 to 50 kHz for the cell made of periodic plane frame elements. Attenuation of at least 18% per cell ($\delta_c \geq 0.18$, light gray), and of at least 67% per cell ($\delta_c \geq 0.67$, dark gray)

4 Conclusions

In the present study, a procedure to model the stochastic response of a three-dimensional phononic crystal and verify its robustness with respect to varying mechanical properties using the estimated distribution via a highly precise MCMC algorithm is proposed. A geometrically periodic three-dimensional frame was simulated and the proposed procedure applied, presenting two robust band gaps: a first one occurring at low frequencies with minimum attenuation of at least 18% per cell for all waves (longitudinal, flexural and torsional) and throughout the IBZ. The second one occurs at high frequencies, presenting some attenuation bands of at least 67% and throughout the IBZ. The deterministic response using constant mechanical properties was simulated using the mean values of the statistical distributions to better interpret the occurring attenuation phenomena, indicating that may have attenuation phenomena other than Bragg scattering band gaps.

Acknowledgements. The authors gratefully acknowledge the financial support of the São Paulo Research Foundation (FAPESP) through processes number 2019/00315-8, 2018/15894-0, and 2014/19054-6, and the Brazilian National Council of Research CNPq (Grant Agreement ID: 420304/2018-5).

Authorship statement. The authors hereby confirm that they are the sole liable persons responsible for the authorship of this work, and that all material that has been herein included as part of the present paper is either the property (and authorship) of the authors, or has the permission of the owners to be included here.

References

[1] Elmadih, W., Chronopoulos, D., Syam, W., Maskery, I., Meng, H., & Leach, R., 2019a. Three-dimensional resonating metamaterials for low-frequency vibration attenuation. *Scientific reports*, vol. 9, n. 1, pp. 1–8.
[2] Elmadih, W., Syam, W. P., Maskery, I., Chronopoulos, D., & Leach, R., 2019b. Multidimensional phononic bandgaps in three-dimensional lattices for additive manufacturing. *Materials*, vol. 12, n. 11, pp. 1878.

[3] Dal Poggetto, V. F. & Serpa, A. L., 2020. Elastic wave band gaps in a three-dimensional periodic metamaterial using the plane wave expansion method. *International Journal of Mechanical Sciences*, pp. 105841.
[4] Fabro, A., Beli, D., Arruda, J., Ferguson, N., & Mace, B., 2016. Uncertainty analysis of band gaps for beams with periodically distributed resonators produced by additive manufacturing. In *ISMA 2020 Conference on Noise and Vibration Engineering. Leuven, Belgium*, volume 12.
[5] Beli, D., Arruda, J., & Ruzzene, M., 2018. Wave propagation in elastic metamaterial beams and plates with interconnected resonators. *International Journal of Solids and Structures*, vol. 139, pp. 105–120.
[6] Ribeiro, L. H. M. S. R., Dal Poggetto, V. F., Beli, D., Frabro, A. T., & Arruda, J. R. F., 2020a. A bayesian approach for modeling the robustness of vibration attenuation bands of two-dimensional periodic frame structures. *Submitted article*, pp. 1–42.
[7] Beli, D., Fabro, A. T., Ruzzene, M., & Arruda, J. R. F., 2019. Wave attenuation and trapping in 3d printed cantilever-in-mass metamaterials with spatially correlated variability. *Scientific reports*, vol. 9, n. 1, pp. 1–11.
[8] Machado, M., Adhikari, S., Dos Santos, J., & Arruda, J., 2018. Estimation of beam material random field properties via sensitivity-based model updating using experimental frequency response functions. *Mechanical Systems and Signal Processing*, vol. 102, pp. 180–197.
[9] Zhang, X., He, J., Takezawa, A., & Kang, Z., 2018. Robust topology optimization of phononic crystals with random field uncertainty. *International Journal for Numerical Methods in Engineering*, vol. 115, n. 9, pp. 1154–1173.
[10] Ribeiro, L. H. M. S., Dal Poggetto, V. F., Beli, D., Fabro, A. T., & Arruda, J. R. F., 2020b. Investigating the influence of mechanical property variability on dispersion diagrams using bayesian inference. In *5th International Symposium on Uncertainty Quantification and Stochastic Modeling (Uncertainties 2020)*.
[11] Ribeiro, L. H. M. S., Dal Poggetto, V. F., Beli, D., Fabro, A. T., & Arruda, J., 2020c. A two-dimensional lattice with band gaps robust to mechanical variability. In *ISMA 2020 Conference on Noise and Vibration Engineering. Leuven, Belgium*, volume 16.
[12] Souza, M. R., Beli, D., Ferguson, N. S., Arruda, J. R. d. F., & Fabro, A. T., 2020. A bayesian approach for wavenumber identification of metamaterial beams possessing variability. *Mechanical Systems and Signal Processing*, vol. 135, pp. 106437.
[13] Tauchert, T. R., 1974. *Energy principles in structural mechanics*. McGraw-Hill Companies.
[14] Kollbrunner, C. F. & Basler, K., 1969. *Torsion in structures: an engineering approach*. Springer Science & Business Media.
[15] Ahmida, K. M. & Arruda, J. R. F., 2001. Spectral element-based prediction of active power flow in timoshenko beams. *International Journal of Solids and Structures*, vol. 38, n. 10-13, pp. 1669–1679.
[16] Black, T. A., 2005. *Spectral element analysis of bars, beams, and Levy plates*. PhD thesis, Virginia Tech.
[17] Hutchinson, J., 2001. Shear coefficients for timoshenko beam theory. *J. Appl. Mech.*, vol. 68, n. 1, pp. 87–92.
[18] Craig, R. R. & Kurdila, A. J., 2006. *Fundamentals of structural dynamics*. John Wiley & Sons.
[19] Leung, A. Y.-T., 1978. An accurate method of dynamic condensation in structural analysis. *International Journal for Numerical Methods in Engineering*, vol. 12, n. 11, pp. 1705–1715.
[20] Floquet, G., 1883. Sur les équations différentielles linéaires à coefficients périodiques. In *Annales scientifiques de l'École normale supérieure*, volume 12, pp. 47–88.
[21] Bloch, F., 1929. Über die quantenmechanik der elektronen in kristallgittern. *Zeitschrift für physik*, vol. 52, n. 7-8, pp. 555–600.
[22] Manconi, E., 2008. *Modelling wave propagation in two-dimensional structures using a wave/finite element technique*. PhD thesis, Universita'di Parma. Dipartimento di Ingegneria Industriale.
[23] Wormser, M., Wein, F., Stingl, M., & Körner, C., 2017. Design and additive manufacturing of 3d phononic band gap structures based on gradient based optimization. *Materials*, vol. 10, n. 10, pp. 1125.
[24] Ribeiro, L. H. M. S. R., Dal Poggetto, V. F., & Arruda, J. R. F., 2020d. Wavenumber identication of periodic one- and two-dimensional structures using prony's method. *Submitted article*, pp. 1–25.
[25] Nogueira, D. A., S. T. & Ferreira, D. F. ., 2004. Avaliação de critérios de convergência univariados para o método de monte carlo. *Revista Brasileira de Estatística*, vol. 65, n. 224, pp. 59–88.
[26] Plummer, M. e. a., 2019. coda: Output analysis and diagnostics for mcmc.
[27] Li, C.-C. & Der Kiureghian, A., 1993. Optimal discretization of random fields. *Journal of engineering mechanics*, vol. 119, n. 6, pp. 1136–1154.
[28] De Cursi, E. S. & Sampaio, R., 2015. *Uncertainty quantification and stochastic modeling with matlab*. Elsevier.
[29] Robert, C., 2007. *The Bayesian choice: from decision-theoretic foundations to computational implementation*. Springer Science & Business Media.
[30] Bathe, K.-J., 2006. *Finite element procedures*. Klaus-Jurgen Bathe.